Ratchet effects induced by terahertz radiation in heterostructures with a lateral periodic potential

P. Olbrich[1], E.L. Ivchenko[2], T. Feil[1], R. Ravash[1], S.D. Danilov[1], J. Allerdings[1], D. Weiss[1], and S. D. Ganichev[1]*
[1] *Terahertz Center, University of Regensburg, 93040 Regensburg, Germany and*
[2] *A.F. Ioffe Physico-Technical Institute, Russian Academy of Sciences, 194021 St. Petersburg, Russia*

We report on the observation of terahertz radiation induced photogalvanic currents in semiconductor heterostructures with one-dimensional lateral periodic potential. The potential is produced by etching a grating into the sample surface. The electric current response is well described by phenomenological theory including both the circular and linear photogalvanic effects. Experimental data demonstrate that the inversion asymmetry of the periodic lateral pattern can be varied by means of electron beam lithography to produce classical lateral ratchets. A novel microscopical mechanism for the polarization-dependent photogalvanic effects has been proposed to interpret the experimental findings. The photocurrent generation is based on the combined action of the lateral periodic potential and the modulated in-plane pumping. The latter modulation stems from near-field effects of the radiation propagating through the grating.

I. INTRODUCTION

Nonequilibrium spatially-periodic noncentrosymmetric systems are able to transport particles in the absence of an average macroscopic force. The directed transport in such systems, generally known as the ratchet effect, has a long history and is relevant for different fields of physics[1,2,3,4,5,6,7,8]. If this effect is induced by electromagnetic radiation it is usually referred to as photogalvanic (or photovoltaic) effect, particularly if breaking of the spatial inversion symmetry is related to the microscopic structure of the system[9,10,11,12,13]. Blanter and Büttiker[14,15] have shown that one of the possible realizations of the Seebeck ratchet can be a superlattice irradiated by light through a mask of the same period but phase shifted with respect to the superlattice. In the present work we have experimentally realized this idea with some modifications. The photocurrent has been observed in semiconductor heterostructures with a one-dimensional lateral periodic potential induced by etching a noncentrosymmetric grating into the sample cap layer. The in-plane modulation of the pump radiation appears hence not via a mask with periodic structures but due to the near-field effects of radiation propagating through the grating. This photothermal ratchet effect was predicted by Büttiker[14] and is polarization independent under normal light incidence. In addition we have observed photocurrents sensitive to the plane of polarization of the linearly polarized terahertz (THz) radiation and to the helicity in case of circularly polarized photoexcitation. The theoretical analysis enables us to propose new mechanisms of the observed circular and linear photogalvanic effects which are related to the combined action of out-of-phase periodic potential and in-plane modulated pumping of the two-dimensional electron system.

*e-mail: sergey.ganichev@physik.uni-regensburg.de

II. SAMPLES AND EXPERIMENTAL METHODS

Here we study photocurrents in (001)-grown GaAs/AlGaAs heterostructures with superimposed lateral grating having a period of 2.5 μm. The electronic micrograph are shown in the inset of Fig. 2. The lateral gratings are prepared on molecular-beam epitaxy (100)-grown Si-δ-doped n-type GaAs/$Al_{0.3}Ga_{0.7}As$ quantum-well structures. The mobility μ and carrier density n_s measured at 4.2 K in our single QW structure of 30 nm width are $\mu = 4.82 \times 10^6$ cm^2/Vs and $n_s = 1.7 \times 10^{11}$ cm^{-2}. Samples grown along $z \parallel [100]$ were square shaped with sample edges of 5 mm length oriented along $[1\bar{1}0]$ and [110]. To measure photocurrents, pairs of ohmic contacts were alloyed in the middle of sample edges. Gratings of 0.5 μm width and period 2.5 μm are obtained by electron beam lithography and subsequent reactive ion etching using $SiCl_4$. Care was taken not to etch through the two-dimensional electron gas. To get a large patterned area of about 1.4 mm^2, 64 squares, each 150μm $\times$ 150 μm, were stitched together. The one-dimensional gratings are oriented either along $\langle 010 \rangle$ (sample A) or close to $\langle 110 \rangle$ (samples B and C) crystallographic directions. In the latter case the grating is slightly misaligned by a small angle of about 4° with respect to the crystallographic direction. While the cross section of grooves prepared close to the $\langle 110 \rangle$ crystallographic direction is rather symmetric the shape of grooves prepared along $\langle 010 \rangle$ crystallographic direction is substantially asymmetric. The average depth on the right side of the groove is smaller than that on the left side. The reason for this might be attributed to the difference in the etching velocities along [110] and $[1\bar{1}0]$ directions[17,18].

For optical excitation we used pulsed molecular THz lasers with NH_3 as an active medium[19]. Circularly and linearly polarized radiation pulses of about 100 ns duration with wavelength λ= 280 μm and power $P \simeq 2$ kW were applied. The photocurrents were induced by indi-

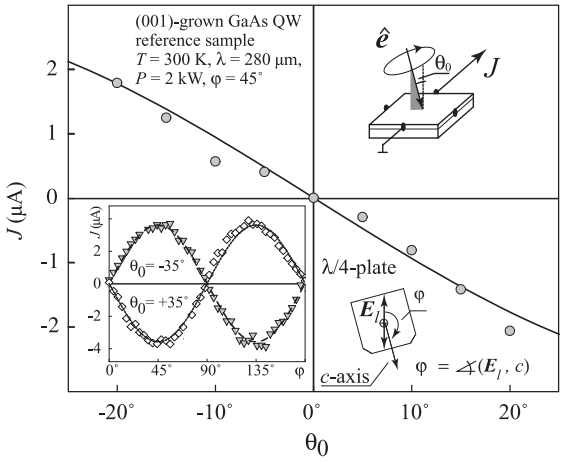

FIG. 1: Circular photogalvanic current $J_C = [J(\varphi = 45^\circ) - J(\varphi = 135^\circ)]/2$ as a function of angle of incidence θ_0 measured in a GaAs/$Al_{0.3}Ga_{0.7}$. As reference QW sample without lateral structure. The current is measured in the direction normal to light propagation. Photocurrent is excited by radiation with wavelength $\lambda = 280$ μm and power $P \approx 2$ kW. The inset (bottom, left) shows the dependence of the total photocurrent J on angle φ measured for angles of incidence $\theta_0 = \pm 35^\circ$. Two other insets (right panels) show, respectively, the experimental geometry and the quarter-wave plate which varies the radiation helicity according to $P_{\rm circ} = \sin 2\varphi$. Full lines are fits to the phenomenological theory for C_{2v} symmetry relevant for (001)-grown unstructured III-V QWs and given by Eq. (1), see[16].

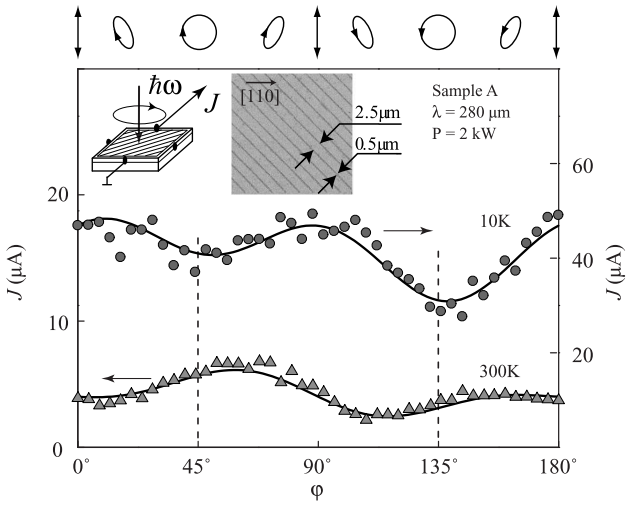

FIG. 2: Photocurrent measured as a function of the angle φ at normal incidence ($\theta_0 = 0^\circ$) in sample A with the asymmetric lateral structure prepared along the [010] crystallographic axis. The current is measured at room temperature and T = 10 K, excited by the radiation with wavelength $\lambda = 280$ μm and power $P \approx 2$ kW. Full line are fits to Eq. (2) (see also Eq. (8)). Left inset shows the experimental geometry, and central inset displays a micrograph of the grating. The ellipses on top illustrate the state of polarization for various angles φ.

rect intrasubband (Drude-like) optical transitions in the lowest size-quantized subband. To measure polarization dependencies we used $\lambda/4$ plates for conversion of linear to circular polarization. The helicity is described by $P_{\rm circ} = \sin 2\varphi$, where φ is the angle between the initial plane of laser beam polarization $\boldsymbol{E}_l$ and the c-axis of the $\lambda/4$ plate. To investigate the photogalvanic effects we also used linearly polarized light. In the experiments the plane of polarization of the radiation, incident on the sample, was rotated by $\lambda/2$ plates. This enabled us to vary the azimuth angle α from 0° to 180° covering all possible orientations of the electric field vector in the interface plane. Radiation was applied at oblique incidence described by the angle of incidence θ_0 varying from -25° to $+25^\circ$ (Fig. 1) and at normal incidence (Fig. 2). The current generated by THz-light in the unbiased samples was measured via the voltage drop across a 50 Ω load resistor in a closed-circuit configuration. The voltage was recorded with a storage oscilloscope.

In (001)-oriented unpatterned samples a signal is only detectable under oblique incidence. The photocurrent measured perpendicularly to the wave vector of the incident light is almost proportional to the helicity P_c and reverses its direction when the polarization switches from left-handed to right-handed circular (see the inset panel of Fig. 1). A photocurrent, but of substantially smaller magnitude, is also generated by applying linearly polarized radiation. In the whole temperature range from room temperature to 4.2 K and for excitation with both circularly as well as linearly polarized radiation the variation of the angle of incidence from θ_0 to $-\theta_0$ changes the sign of the photocurrent J. This is shown in Fig. 1 for the circular photogalvanic effect (CPGE) obtained after $J_C = [J(\varphi = 45^\circ) - J(\varphi = 135^\circ)]/2$. For normal incidence the photocurrent vanishes. The photocurrent is well described by the phenomenological theory of the circular and linear photogalvanic effect obtained for the point group C_{2v} which is relevant for this type of structures[20]. Theory yields for the dominating CPGE photocurrent $J_{\rm ref}$ of the unpatterned reference sample:

$$J_{\rm ref} = a_{\rm ref} \sin\theta_0 \xi P_c \,, \qquad (1)$$

where $a_{\rm ref}$ is a constant, $\xi = t_p t_s / t_0^2$, t_p and t_s are the Fresnel transmission coefficients for the p- and s-polarized light, respectively, and t_0 is the transmission coefficient under normal incidence. The corresponding fits of our data are shown in Fig. 1 by the full line and in the inset in Fig. 1 as dashed and dotted lines.

The situation changes drastically for samples with grating. Now a photocurrent is also detected at normal incidence. The width of the photocurrent pulses is about 100 ns which corresponds to the THz laser pulse duration. In the patterned samples with the grooves oriented along $\langle 010 \rangle$ we observed that the magnitude of the photocurrent detected at normal incidence (Fig. 2) is comparable and even larger than that obtained in the reference sample at large angles of incidence (Fig. 1). Moreover the

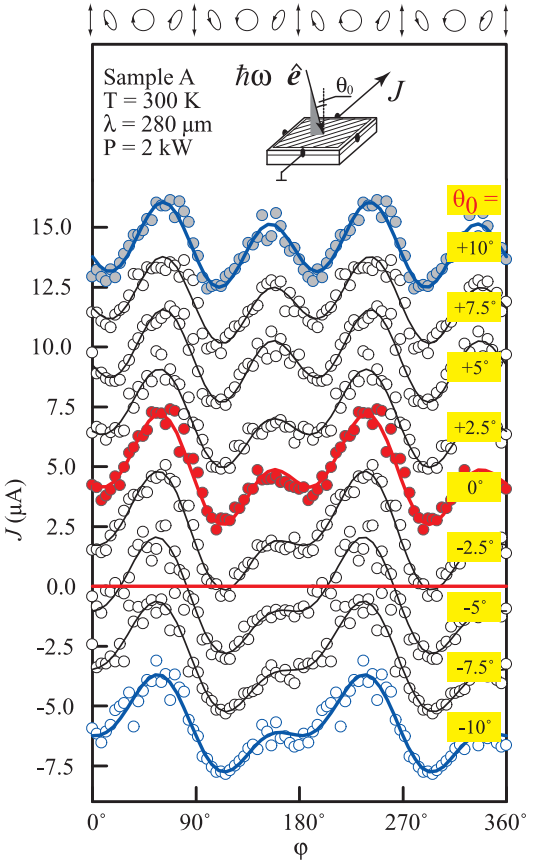

FIG. 3: Photocurrent measured as a function of the angle φ at various angles of incidence (θ_0) in sample A with an asymmetric lateral structure prepared along the [010] crystallographic axis. The data for $\theta_0 \neq 0$ are shifted by $+2.5$ μA for each 2.5° step (positive θ_0) and by -2.5 μA for each 2.5° step (negative θ_0). The current is measured at room temperature, excited by radiation with wavelength $\lambda = 280$ μm and power $P \approx 2$ kW. Full lines are fits to Eqs. (2) (see also Eq. (8)). The inset shows the experimental geometry. The ellipses on top illustrate the state of polarization for various angles φ. The data, periodic in π, are plotted from $\varphi = 0°$ to $\varphi = 360°$ to better visualize the features of interest.

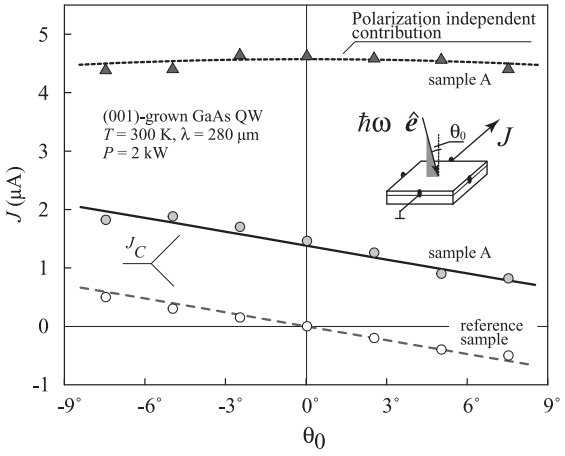

FIG. 4: Circular photogalvanic current $J_C = [J(\varphi = 45°) - J(\varphi = 135°)]/2$ measured as a function of the incidence angle θ_0 in sample A with the asymmetric lateral structure along [010] crystallographic axis (full circles) and the unstructured reference QW sample (open circles). The current is measured in the direction normal to light propagation and excited by radiation with wavelength $\lambda = 280$ μm and power $P \approx 2$ kW. Full and dashed lines are fits to Eqs. (3), see also the term proportional to P_c in Eq. (8), and (1), respectively. Triangles show the θ_0 dependence of the polarization-insensitive photocurrent together with the curve calculated according to $J = d\xi \cos\theta_0$ following from Eq. (6). The data are obtained from fitting the φ-dependence of the photocurrent J taken at various incidence angles. Inset shows the experimental geometry used for sample A.

polarization behaviour has changed. Figure 2 shows ellipticity dependent measurements of sample A excited at normal incidence. The data can be well fitted by

$$J = a \sin 2\varphi + b \sin 4\varphi + c \cos 4\varphi + d\,. \qquad (2)$$

Here, the parameters a, b, c, and d are phenomenological fitting parameters, described below. Figure 2 shows that the photon helicity dependent photocurrent caused by circular photogalvanic effect gives an essential contribution. Figure 4 displays the CPGE current as a function of the angle of incidence θ_0 for sample A (open circles) and the unstructured reference sample (full circles). To extract the CPGE current from the total current we used the fact that the CPGE contribution, given by the term $a \sin 2\varphi$, changes its sign upon switching the helicity while all the other terms remain unchanged. Taking the difference of photocurrents of right and left handed radiation we get the CPGE current J_C. At oblique incidence, in the structured sample it consists of two contributions. The first one has the same origin as the one observed in the reference sample and is described by Eq. (1). The second one is due to the lateral structure. The dependence of the CPGE photocurrent on the angle of incidence θ_0 can be well fitted by

$$J_C = (a_{\rm ref} \sin\theta_0 + a \cos\theta_0)\xi\,. \qquad (3)$$

Now we turn to the photon helicity independent contributions to the photocurrent, denoted by coefficients b, c and d in Eq. (2). These contributions we attribute to the linear photogalvanic effect (LPGE). The LPGE photocurrents can be generated by applying linearly polarized radiation. Figure 5 shows the dependence of the photocurrent on the azimuth angle describing the variation of the light's electric field direction relative to the crystallographic direction [110]. We found that all data can be well fitted by

$$J = 2b \sin 2\alpha + 2c \cos 2\alpha + d - c\,. \qquad (4)$$

We emphasize that b, c, and d are the same fitting parameters used for the data shown in Fig. 2. Figure 4 shows the dependence of the polarization independent contribution, proportional to the coefficient d, on the angle of

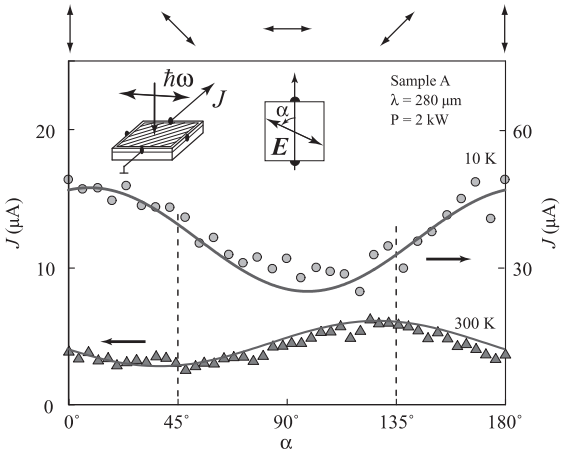

FIG. 5: Photocurrent J measured as a function of the angle α under normal incidence at room temperature and T = 10 K in sample A with the asymmetric lateral structure along [010] crystallographic axis. Photocurrent is excited by linearly polarized radiation with wavelength $\lambda = 280$ μm and power $P \approx 2$ kW. Full lines are fits to Eq. (4), see also Eq. (9). We used for fitting the same values of b, c and d as in the experiments with elliptically polarized radiation, see Fig. 2. Left inset shows the experimental geometry, and right inset defines the angle α. On top the arrows indicate the polarization corresponding to various values of α.

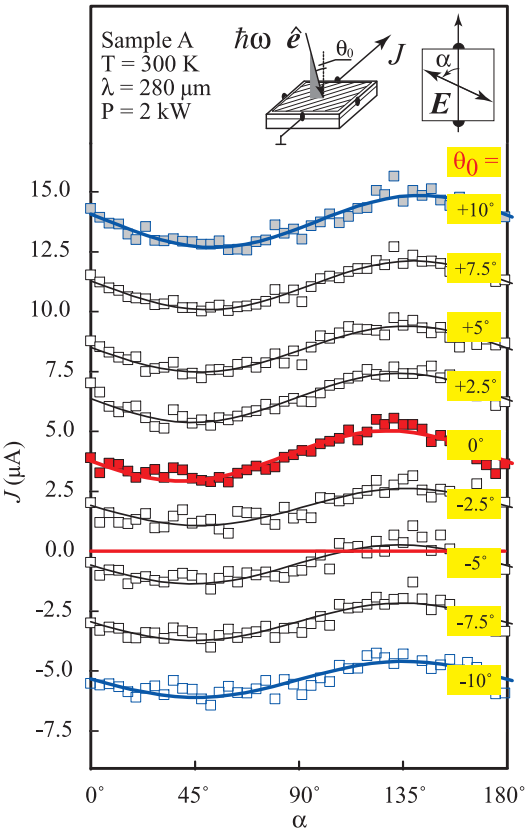

FIG. 6: Photocurrent J measured as a function of the angle α at room temperature in sample A with the asymmetric lateral structure along [010] crystallographic axis. The data for $\theta_0 \neq 0$ are shifted by $+2.5$ μA for each 2.5° step (positive θ_0) and by -2.5 μA for each 2.5° step (negative θ_0). The current is measured at room temperature, excited by radiation with wavelength $\lambda = 280$ μm and power $P \approx 2$ kW. Full lines are fits to Eqs. (2), see also Eq. (9). The left inset shows the experimental geometry. The right inset displays the sample and the radiation electric field viewing from the source of radiation side.

incidence θ_0. In this case the experimental data can be well fitted by

$$J = d \cos\theta_0 \xi \,. \tag{5}$$

Figures 2 and 5 demonstrate that the dominant contribution to the photocurrent is polarization independent and can therefore be obtained by unpolarized radiation. In samples B and C with the grooves oriented along ⟨110⟩ crystallographic directions we also detected a photocurrent at normal incidence having the same polarization dependences as sample A, Eqs. (2) and (4). However, the photocurrent measured in sample A is about an order of magnitude larger than in sample B and C. We ascribe this to the grooves profile being strongly asymmetric in sample A while nearly symmetric in samples B and C.

III. PHENOMENOLOGICAL DESCRIPTION

In this section our theoretical analysis of the experimental data is based on the symmetry considerations of the phenomenological equations describing the photogalvanic effects (PGE) under study. Under normal incidence of the laser radiation on the sample the in-plane photocurrent is given by

$$j_l = I \sum_{m,n} \chi_{lmn} \{e_m e_n^*\} + I \gamma_{lz} P_c \,, \tag{6}$$

where l, m, n are the in-plane coordinates, $\{e_m e_n^*\} = (e_m e_n^* + e_n e_m^*)/2$, I, $\boldsymbol{e}$ and P_c are the light intensity, polarization unit vector and degree of circular polarization. The third rank tensor χ_{lmn} describing the linear PGE is symmetrical with respect to the interchange of the second and third indices, and γ_{lm} is a second-rank pseudotensor describing the circular PGE. The (001)-grown heterostructure has the point-group symmetry $F_{\rm ref} = C_{2v}$ which forbids in-plane photocurrents under normal incidence[19] as it is confirmed by measurements performed on the reference samples.

The lateral superlattice can reduce the symmetry of the system. Let us denote the superimposed periodic lateral potential as $V(\boldsymbol{\rho})$, where $\boldsymbol{\rho}$ is the two-dimensional radius-vector, and introduce the period a and two in-plane axes x and y oriented, respectively, parallel and perpendicular to the direction of periodicity. Then, by definition, the lateral superlattice potential does not depend on y and is a periodic function of x, namely, $V(x + a) = V(x)$. One of the symmetry elements of this potential is the mirror reflection plane σ_y perpendicular

to the axis y. Its total point-group symmetry $F_{\rm SL}$ can be either C_s if the function $V(x)$ is asymmetric or C_{2v} if $V(x)$ is an even function with respect to a certain origin on the axis x. In the latter case, in addition to the identity element e and the mirror plane σ_y, the point group contains the mirror plane $\sigma_x \perp x$ and the second-order rotation axis $C_2 \parallel z$.

The symmetry of the structured sample is determined by the direct product $F_{\rm ref} \times F_{\rm SL}$ of the point groups describing the symmetries of the reference heterostructure and lateral potential. If the potential $V(x)$ is symmetrical both groups $F_{\rm ref}$ and $F_{\rm SL}$ have a common element C_2 and the photocurrents under normal incidence are forbidden. This is obviously realized in the samples with the superlattice axes x, y oriented in the $\langle 110 \rangle$ directions. Thus, the photocurrents can be induced under normal incidence only in the case of an asymmetrical potential $V(x)$. If the axes x, y of this potential coincide with the axes $[1\bar{1}0]$, $[110]$, the symmetry of the system is C_s, Eq. (6) reduces to

$$\begin{aligned} j_x &= I[\chi_1 + \chi_2(|e_x|^2 - |e_y|^2)]\,, \\ j_y &= 2I\chi_3\{e_x e_y^*\} + I\gamma P_c\,, \end{aligned} \tag{7}$$

and is governed by four linearly independent coefficients. If the axes x, y are rotated with respect to $[1\bar{1}0]$, $[110]$ by an angle different from multiples of 90° the structured sample lacks any symmetry operations except for the identity and corresponds to the point group C_1. Phenomenologically, in this case each of the photocurrents component j_x, j_y is a sum of a polarization-independent term and three terms proportional to $|e_x|^2 - |e_y|^2, \{e_x e_y^*\}$ and P_c, and the normal-incidence PGE is described by eight independent coefficients.

Equations (7) describe the normal-incident photocurrent for any in-plane orientation of the axes x, y if the microscopic asymmetry of an unstructured quantum well is ignored and only asymmetry of the lateral superlattice is taken into account. If the pair of contacts makes an angle of 45° with the axes x and y the normal-incidence photocurrent is an equal superposition of the currents j_x and j_y. If the initial laser light is polarized along the line l connecting the contacts then, for normal incidence, the dependence of the photocurrent component j_l along this line on the orientation of the $\lambda/4$ and $\lambda/2$ plates is given by

$$j_l(\varphi)/I = \gamma_l \sin 2\varphi + \frac{\chi_{3l}}{2}\sin 4\varphi + \frac{\chi_{2l}}{2}\cos 4\varphi + \chi_{1l} + \frac{\chi_{2l}}{2}\,, \tag{8}$$

and

$$j_l(\alpha)/I = \chi_{3l}\sin 2\alpha + \chi_{2l}\cos 2\alpha + \chi_{1l}\,, \tag{9}$$

respectively. These equations agree with the experimental polarization dependences of the current $J \propto j_l$ [see Figs. 2, 5 and Eqs. (2), (4)] yielding

$$\gamma_l = a, \qquad \frac{\chi_{3l}}{2} = b, \qquad \frac{\chi_{2l}}{2} = c, \qquad \chi_{1l} = d - c\,.$$

The dependence of the photocurrent j_l on the angle of incidence θ_0 can be described by the factor $\cos\theta_0\xi$. This also agrees with experimental observations which are well fitted by Eqs. (5) and (3), see Fig. 4 which shows the CPGE and LPGE contributions given by coefficients a and d, respectively.

An additional mechanism of the asymmetry leading to the photocurrents can be related to the space-modulated intensity of the radiation exciting the structure. Such an inhomogeneous distribution of the electric field in structured samples with distance between the groove edges and QW layers of nanometer scale is expected due to near-field effects. In the THz range a local enhancement of electric fields in structures with subwavelength pattern has previously been observed in GaAs tunnelling Schottky barrier junctions (for review see Chapter 2 in the book[19]). In our samples, due to the near-field effects, the amplitude of a plane electromagnetic field penetrating through the superimposed grating becomes a periodic function of x with the same period a. In the asymmetrical structure the potential $V(x_c)$ and the intensity $I(x_c)$ of the normally-incident radiation can be shifted relative to each other in phase. As a result, the product $I(x_c)(dV/dx_c)$ averaged over space as well as the coefficients χ_j in Eq. (7) are nonvanishing.

IV. MICROSCOPICAL MODEL

If the lateral superstructure is responsible for the PGE observed at normal incidence then one can ignore the initial symmetry C_{2v} of the reference heterostructure, disregard mechanisms of PGE related to the lack of an inversion center in the unstructured sample and rely only on the symmetry of superstructure potential $V(x)$ and the in-plane intensity modulation. In this case one can apply Eqs. (7) for any orientation of the axes x, y irrespectively to the crystallographic directions $[1\bar{1}0]$, $[110]$.

We have analyzed microscopic mechanisms of PGE by using the classical Boltzmann equation for the electron distribution function $f_{\boldsymbol{k}}$, namely,

$$\left(\frac{\partial}{\partial t} + v_{\boldsymbol{k},x}\frac{\partial}{\partial x} + \frac{\boldsymbol{F}}{\hbar}\frac{\partial}{\partial \boldsymbol{k}}\right) f_{\boldsymbol{k}}(x) + Q_{\boldsymbol{k}}^{(p)} + Q_k^{(\varepsilon)} = 0\,. \tag{10}$$

Here the simplified notation x is used for the coordinate x, $\boldsymbol{k}$ is the electron two-dimensional wave vector, $\boldsymbol{F}$ is a sum of the time-dependent electric-field force

$$e\boldsymbol{E}(t) = e(\boldsymbol{E}_0 e^{-i\omega t} + \boldsymbol{E}_0^* e^{i\omega t}) \tag{11}$$

of the light wave and the static force $-dV(x)/dx$, ω is the light frequency, $\boldsymbol{v}_{\boldsymbol{k}} = \hbar\boldsymbol{k}/m^*$ is the electron velocity, e and m^* are the electron charge and effective mass, $Q_{\boldsymbol{k}}^{(p)}$ and $Q_k^{(\varepsilon)}$ are the collision terms responsible for the electron momentum and energy relaxation, respectively. The operator $Q_{\boldsymbol{k}}^{(p)}$ is taken in the simplest form

$$Q_{\boldsymbol{k}}^{(p)} = \frac{f_{\boldsymbol{k}} - \langle f_{\boldsymbol{k}}\rangle}{\tau}\,, \tag{12}$$

where τ is the momentum relaxation time and the brackets mean averaging over the directions of $\boldsymbol{k}$. The operator $Q_k^{(\varepsilon)}$ acts on the distribution function averaged over the directions of $\boldsymbol{k}$ and depends only on the modulus $k = |\boldsymbol{k}|$. Equation (10) is valid for the weak and smooth potential satisfying the conditions $|V(x)| \ll \varepsilon_e$ and $q_0 \equiv 2\pi/a \ll k_e$, where k_e and ε_e are the typical electron wave vector and energy, and for the photon energy $\hbar\omega$ being much smaller than ε_e.

If the space modulation of the radiation intensity is ignored the photocurrent is obtained by solving Eq. (10) in the fifth order perturbation theory, namely, the second order in the amplitude of the light electric field $\boldsymbol{E}_0$ and the third order in the lateral potential $V(x)$

$$j_l = R_l |\boldsymbol{E}_0|^2 \overline{\left(\frac{dV}{dx}\right)^3} \equiv R_l |\boldsymbol{E}_0|^2 \zeta (q_0 \tilde{V})^3 \,. \qquad (13)$$

Here $\tilde{V}^2$ is the dispersion $\overline{V(x)^2}$, the overline means averaging over space (without losing generality, we suppose $\overline{V(x)} = 0$), and ζ is a dimensionless measure of the potential asymmetry. For the simplest asymmetric potential $V_1 \cos(q_0 x) + V_2 \sin(2q_0 x)$ with $q_0 = 2\pi/a$, the parameter ζ equals $-3\sqrt{2}V_1^2 V_2/(V_1^2+V_2^2)^{3/2}$ and $\tilde{V}^2 = (V_1^2+V_2^2)/2$. The form of the coefficient R_l in Eq. (13) depends on the radiation polarization, in accordance with Eq. (7), and the experimental conditions, particularly, on the relation between the light frequency ω and the momentum and energy relaxation times, τ and τ_ε, respectively, as well as on the relation between the period a and the electron free-path length l_e and energy diffusion length l_ε.

V. ESTIMATIONS FOR PHOTOGALVANIC CURRENTS

Circular PGE. First of all, we present an estimation for the circular photocurrent described by the coefficient γ in the second equation (7) for the non-degenerate electron gas in the limiting case $\tau_\varepsilon^{-1}, q_0 l_e, q_0 l_\varepsilon \ll \omega$:

$$j_y = \gamma I \approx e\nu g \tau N \frac{\hbar k_e}{m^*} \left(\frac{q_0}{k_e}\right)^3 \frac{\zeta \tilde{V}^3}{k_B T (\hbar\omega)^2} \,, \qquad (14)$$

where $\nu = d\ln\tau/d\ln\varepsilon$, g is the photon absorption probability rate per particle:

$$g = \frac{4\pi e^2}{m^* c n_\omega} \frac{I}{\hbar\omega} \frac{\tau}{1+(\omega\tau)^2} \,. \qquad (15)$$

The radiation intensity I is related to the amplitude $\boldsymbol{E}_0$ by

$$I = \frac{c n_\omega}{2\pi} (|E_{0x}|^2 + |E_{0y}|^2) \,,$$

n_ω is the refraction index and c is the light velocity in vacuum. While deriving Eq. (14) we assumed g to be x-independent.

Polarization-independent PGE. The photocurrent independent of polarization and proportional to the coefficient χ_1 in Eq. (7) can be related to heating of free carriers by the electromagnetic wave. At high temperatures the conditions $l_e, l_\varepsilon \ll a$ are fulfilled, and the kinetic equation (10) can be reduced to the macroscopic equations for the two-dimensional electron density $N(x)$, local nonequilibrium temperature $\Theta(x)$, current density j_x and energy flux density $i_{\varepsilon,x}(x)$. In the continuity equation for the energy flux density the supplied and dissipated powers are taken in the form

$$W_\varepsilon^{(\mathrm{in})} = \hbar\omega g N \,,\; W_\varepsilon^{(\mathrm{out})} = \frac{k_B(\Theta - T)}{\tau_\varepsilon} \, N \,, \qquad (16)$$

where τ_ε is the energy relaxation time, Θ is the local electron temperature, T is the equilibrium phonon temperature and k_B is the Boltzmann constant. In what follows we assume a moderate pump power resulting in a weak increase in the temperature, $\Theta - T \ll T$. Under the homogeneous optical excitation the macroscopical equations have the following solution

$$k_B\Theta = k_B T + \hbar\omega g \tau_\varepsilon \,,\; N(x) = N_0 \mathrm{e}^{-V(x)/k_B\Theta} \,,$$

where N_0 is x-independent. For this solution both the electric current j_x and the flux $i_{\varepsilon,x}$ are absent. However, a value of j_x becomes nonzero with allowance for the generation rate g to vary in space. Let this variation be described by $g(x) = g_0 + g^{(1)} \cos(q_0 x + \varphi_g)$. The steady-state inhomogeneous generation produces a permanent periodic electron temperature

$$k_B\Theta(x) = k_B T + \tau_\varepsilon \hbar\omega g^{(1)} \cos(q_0 x + \varphi_g)$$

which is followed by a light-induced correction to the space-oscillating contribution to the electron density

$$\delta N(x) = -\frac{N_0 \tau_\varepsilon}{k_B T} \hbar\omega g^{(1)} \cos(q_0 x + \varphi_g) \,.$$

The photocurrent is calculated as an average

$$j_x = -\mu \overline{\frac{dV(x)}{dx} \delta N(x)} \,,$$

where u is the mobility $e\tau/m^*$. For the lateral potential taken in the form $V(x) = V_1 \cos(q_0 x + \varphi_V)$, the symmetry of the system is broken due to a phase shift between $V(x)$ and $\Theta(x)$. The result for χ_1 reads

$$\begin{aligned} j_x = \chi_1 I &= \mu N_0 q_0 V_1 \frac{\hbar\omega g^{(1)} \tau_\varepsilon}{2k_B T} \sin(\varphi_g - \varphi_V) \qquad (17) \\ &= \mu N_0 \hbar q_0 \zeta' g_0 \frac{V_1}{2k_B T} \omega\tau_\varepsilon \,. \end{aligned}$$

Here $\zeta' = (g^{(1)}/g_0)\sin(\varphi_g - \varphi_V)$ is the parameter of asymmetry related to the inhomogeneous photoexcitation. The model used to derive Eq. (17) is similar to the model considered in Refs.[14,15] for a ratchet with sinusoidal potential and temperature and a relative phase

lag between them. The difference is that here we assume $V_1 \ll k_BT$ while in Ref.[14] the opposite case is considered. It should be noted that the nonequilibrium asymmetric systems with both a periodic potential $V(x)$ and a periodic temperature profile $T(x)$ are referred to as the Seebeck ratchets[1].

It follows from Eqs. (15) and (17) that microscopically the coefficient χ_1 can be presented in the form

$$\chi_1 = \frac{2\pi e^2}{\hbar c n_\omega}\zeta' \mu N_0 \frac{\hbar q_0}{m^*}\frac{\tau\tau_\varepsilon}{1+(\omega\tau)^2}\frac{V_1}{k_BT}\,. \qquad (18)$$

Circular PGE under inhomogeneous excitation. Now we show that the polarization-dependent photocurrents and even the CPGE currents can as well be induced in a lateral superlattice with the out-of-phase periodic potential $V(x)$ and generation $g(x)$. The photocurrent in the y direction is calculated according to

$$j_y = \frac{2e^2\tau}{m^*}\mathrm{Re}\{\overline{E^*_{0y}(x)\delta N_\omega(x)}\}\,, \qquad (19)$$

where $\delta N_\omega(x)$ is the amplitude of the electron density oscillation linear in the THz electric field E_{0x}. From the continuity equation $-\mathrm{i}\omega e\delta N_\omega + dj_{x,\omega}/dx = 0$ and the equation for the linear-response electric current contribution modulated in space

$$j_{x,\omega} = -\frac{e^2\tau N_0}{m^*}\frac{E_{0x}}{1-\mathrm{i}\omega\tau}\frac{V(x)}{k_BT}$$

we find the amplitude $\delta N_\omega(x)$ and, finally, the circular photocurrent

$$\gamma I = \mu N_0 \hbar q_0 \zeta' g_0 \frac{V_1}{4k_BT}\,. \qquad (20)$$

The coefficient γ is given by

$$\gamma = \frac{\pi e^2}{\hbar c n_\omega}\zeta' \mu N_0 \frac{\hbar q_0}{m^*}\frac{\tau}{\omega(1+\omega^2\tau^2)}\frac{V_1}{k_BT}\,. \qquad (21)$$

The generation of a steady-state electron flow along the y axis sensitive to the circular polarization P_c results from two phase shifts of the oscillation $\delta N(x,t)$, in space with respect to $V(x)$ by $\varphi_g - \varphi_V$ and in time with respect to $E_x(t)$ by $\arctan(\omega\tau)$. This current is smaller as compared with the polarization-independent current by a factor of $2\omega\tau_\varepsilon$. This agrees with the experiment where the polarization-independent contribution is dominating. The ratio of the circular photocurrents (14) and (20) equals $(\zeta/\zeta')(q_0\tilde{V}/k_e\hbar\omega)^2$. Due to the small parameter $(q_0/k_e)^2$ the contribution (20) is expected to exceed the alternative contribution (14). For the inhomogeneous photoexcitation, the coefficients χ_2 and χ_3 have the same order of magnitude $\sim \gamma\omega\tau$.

VI. SUMMARY

A new mechanism of circular and linear photogalvanic effects has been proposed and demonstrated experimentally. The lateral grating etched into the sample's surface induces a periodical lateral potential acting on the two-dimensional electron gas. In addition, it modifies the normally-incident radiation causing its spatial modulation in plane of the electron gas. If the lateral structuring is asymmetrical the spatial modulations of the static lateral potential $V(x)$ and the radiation intensity $I(x)$ are relatively shifted relatively to each other. As a result the product of the static force $-dV(x)/dx$ and the photothermal modulation of the electron density $\delta N(x)$ has a nonzero space average and, therefore, a homogeneous electric current is generated, an effect previously predicted by Blanter and Büttiker[14]. In this paper we have proposed polarization-dependent photocurrents arising in the same system with broken symmetry due to the phase shift between periodic potential and periodic light field. These currents, in contrast to the polarization-independent photocurrent, are independent of the energy relaxation time, if $\omega\tau_\varepsilon \gg 1$, and controlled only by momentum relaxation time.

Acknowledgments

The financial support from the DFG and RFBR is gratefully acknowledged. E.L.I. thanks DFG for the Merkator professorship. We are grateful M.M. Voronov, V.V. Bel'kov, L.E. Golub and S.A. Tarasenko for fruitful discussions.

[1] P. Reimann, Phys. Rep. **361**, 57 (2002).
[2] H. Linke (ed.), *Ratchets and Brownian Motors: Basic Experiments and Applications*, special issue Appl. Phys. A: Mater. Sci. Process. A **75**, 167 (2002).
[3] P. Hänggi, F. Marchesoni, and F. Nori, Ann. Phys. (Leipzig) **14**, 51 (2005).
[4] P. Reimann, M. Grifoni, and P. Hänggi, Phys. Rev. Lett. **79**, 10 (1997).
[5] A. Lorke, S. Wimmer, B. Jager, J.P. Kotthaus, W. Wegscheider, and M. Bichler, Physica B **249-312**, 312 (1998)
[6] H. Linke, T.E. Humphrey, A. Lofgren, A.O. Sushkov, R. Newbury, R.P. Taylor, and P. Omling, Science 286, 2314 (1999).
[7] A.M. Song, P. Omling, L. Samuelson, W. Seifert, and I. Shorubalko, H. Zirath, Appl. Phys. Lett. **79**, 1357 (2001).
[8] J.B. Majer, J. Peguiron, M. Grifoni, M. Tusveld, and J.E. Mooij, Phys. Rev. Lett. **90**, 056802 (2003).

[9] L.I. Magarill, Physica E (Amsterdam) **9**, 652 (2001).
[10] M.V. Entin and L.I. Magarill, Phys. Rev. B **73**, 205206 (2006).
[11] A.D. Chepelianskii, Eur. Phys. J. B **52**, 389 (2006).
[12] A.D. Chepelianskii, M.V. Entin, L.I. Magarill, and D.L. Chepelyansky, Eur. Phys. J. B **56**, 323 (2007); cond-mat/0701128; Physica E (Amsterdam) **40**, 1264 (2008).
[13] W. Weber, L.E. Golub, S.N. Danilov, J. Karch, C. Reitmaier, B. Wittmann, V.V. Bel'kov, E.L. Ivchenko, Z.D. Kvon, N.Q. Vinh, A.F.G. van der Meer, B. Murdin, and S.D. Ganichev, Phys. Rev. B **77** 245304 (2008).
[14] M. Büttiker and Y.M. Blanter, Phys. Rev. Lett. **81**, 4040 (1998).
[15] M. Büttiker, Z. Phys. B **35**, 177 (1979).
[16] E. L. Ivchenko, *Optical Spectroscopy of Semiconductor Nanostructures* (Alpha Science International, Harrow, UK, 2005).
[17] S. Adachi and K. Oe, J. Electrochem. Soc. **130**, 2427 (1983).
[18] S. Adachi, Jap. J. Appl. Phys. **30**, 1196 (1991).
[19] S. D. Ganichev and W. Prettl, *Intense Terahertz Excitation of Semiconductors* (Oxford University Press, Oxford, 2006).
[20] S.D. Ganichev, S.N. Danilov, J. Eroms, W. Wegscheider, D. Weiss, W. Prettl, and E. L. Ivchenko,, Phys. Rev. Lett. **86**, 4358 (2001).
[21] P.S. Kireev, *Semiconductor physics* (Mir Publishers, Moscow 1974).